IEEE Open Journal of
Power Electronics

Received 6 May 2025; revised 5 January 2026; accepted 12 February 2026. Date of publication 16 February 2026;
date of current version 6 March 2026. The review of this article was arranged by Associate Editor Dehong Mark Xu.

Digital Object Identifier 10.1109/OJPEL.2026.3665278

Partial Discharge Mitigation of Medium-Voltage, Medium-Frequency Dry-Type Transformers Using Semiconductive Screening

REZA MIRZADARANI (Graduate Student Member, IEEE), ZHENGZHAO LI (Graduate Student Member, IEEE), ZIAN QIN (Senior Member, IEEE), PETER VAESSEN (Member, IEEE), PAVOL BAUER (Senior Member, IEEE), AND MOHAMAD GHAFFARIAN NIASAR (Member, IEEE)

Department of Electrical Sustainable Energy, TU Delft, 2628 Delft, Netherlands

CORRESPONDING AUTHOR: MOHAMAD GHAFFARIAN NIASAR (e-mail: M.Ghaffarianniasar@tudelft.nl)

This work was supported by the RVO MOOI (Missiegedreven Onderzoek Ontwikkeling en Innovation) under Grant Agreement MOOI 52103.

ABSTRACT This paper presents a practical approach to reduce the size of medium-frequency, medium-voltage dry-type transformers through the innovative use of semiconductive screening. The proposed method minimizes the required air gaps, a critical aspect of dry-type transformer design, particularly for medium-frequency applications. Analytical approaches and Finite Element Method (FEM) simulations in COMSOL are used to demonstrate how to achieve a uniform electric field distribution within the transformers. Experimental investigations by means of partial discharge measurement on a prototype epoxy-based stress cone termination with a semiconductive shield are conducted. The results demonstrate the potential for this method to enhance transformer performance and provide a foundation for further advancements in medium-frequency transformer design.

INDEX TERMS Dry-type transformer, epoxy resin, medium-frequency, medium-voltage, partial discharge, semiconductive screening.

I. INTRODUCTION

Dry-type transformers offer several advantages over oil-immersed transformers, such as reduced fire hazards, minimal maintenance requirements due to the absence of oil, lower operational costs, and minimized environmental risks associated with oil leakage. Their robust design also provides high mechanical strength against short circuit forces. These features make dry-type transformers particularly suitable for densely populated or environmentally sensitive areas. However, the design of the insulation system of a dry-type transformer and the prevention of partial discharges (PDs) are challenging, particularly in high-voltage, medium-frequency applications [1], [2].

One of the key advantages of dry-type transformers in medium-frequency Solid-State Transformer (SST) applications lies in their structural design properties, which help reduce frequency-related losses. In oil-type transformers, the presence of a metallic tank becomes a critical factor affecting energy efficiency at higher frequencies. Increasing frequency raises stray losses, primarily due to eddy currents in the tank. These eddy currents, induced in the conductive material of the tank, cause extra heat, reducing overall efficiency and potentially leading to overheating issues. In contrast, dry-type transformers inherently avoid these frequency-induced stray losses by lacking an oil tank, a key advantage in medium-frequency SST applications. Without a conductive tank, the formation of eddy currents and stray losses are significantly reduced, resulting in more efficient operation in higher-frequency environments.

The insulation in a dry-type transformer consists of solid materials such as epoxy resins and several air gaps between primary and secondary, windings and core, and between phases. The primary purpose of these gaps is to provide electrical insulation and to prevent dielectric breakdown between

TABLE 1. The Geometrical Information of Several Dry-Type Power 50 Hz Transformers

P[1]	V_{HV}[2]	V_{LV}[2]	r_{core}[3]	r_{LVis_in}[4]	r_{LVis_out}[5]	r_{HVis_in}[4]	LV-Core Gap	HV-LV Gap
kVA	kV	V	mm	mm	mm	mm	mm	mm
160	6	400	97.5	101	128.5	165	3.5	36.5
250	6	400	97.5	101	128.5	165	3.5	36.5
300	13.2	220	104.7	110	135.4	170	5.4	34.6
315	11	433	105.5	110	135.4	170	4.5	34.6
400	10	400	105.5	110	135.4	170	4.5	34.6
500	11	433	123.5	127	154.5	190	3.5	35.5
630	10.8	400	123.5	127	154.5	190	3.5	35.5
750	11	415	124.5	128	158.3	195	3.5	36.7
800	6	400	124.5	128	158.3	195	3.5	36.7
1000	10.8	400	121	124.5	158.8	195	3.5	36.2
1250	10.8	400	130	136.5	173.4	215	6.5	41.6
1500	11	415	142	146.5	198.7	235	4.5	36.3
1600	10.8	400	142	146.5	198.7	235	4.5	36.3
2000	10	400	145.8	149	202.2	240	3.2	37.8
2500	6	400	162.5	166	217.1	260	3.5	42.9
3150	6	400	162.5	166	217.1	260	3.5	42.9

[1] P: rating power.
[2] V_{HV} and V_{LV}: the rating voltage of the HV and LV windings, respectively.
[3] r_{core}: the radius of the core.
[4] r_{LVis_in} and r_{HVis_in}: the inner radius of insulation of LV and HV windings, respectively.
[5] $r_{LVis\ out}$: the outer radius of LV winding.

the HV and LV windings and between the windings and the core. The gap size depends on the voltage level and the dielectric strength of the surrounding medium (air). Moreover, adequate gaps facilitate cooling and heat dissipation. Since dry-type transformers rely on natural or forced air cooling, appropriate spacing is essential to ensure a proper heat transfer. The window gaps must maintain mechanical stability and withstand vibrations or movements during operation and transportation. Table 1 summarizes the dimensional information of several dry-type power 50 Hz transformers and shows thermal and mechanical factors influencing the gap between the low-voltage (LV) winding and the core. Nevertheless, thermal and insulation considerations are critical for the gap between high-voltage (HV) and low-voltage (LV) windings. The transformers summarized in Table 1 represent practical dry-type, line-frequency units widely used in industrial and renewable energy applications. These data points are included to provide realistic reference values for insulation dimensions, rather than experimental or downscaled prototypes.

Utilizing semiconductor screens to encapsulate conductors and the insulation system is a well-known practice in the field of high-voltage (HV) and extremely high-voltage (EHV) cable technologies [3]. This approach typically involves triple extrusion, where insulation and semiconductive layers are extruded around the conductor in a single operation. After extrusion, the conductor is covered with a semiconductive layer, an insulation layer, and another semiconductive layer around the insulation. This configuration ensures a robustly bonded interface between the conductor and the dielectric, and addressing potential issues that might arise during thermal cycling, such as separating the insulation layer from the conductor or the metallic screen and forming gaps. These gaps can lead to electric field enhancement, partial discharge initiation, and eventually, cable failure. Additionally, this method prevents the intensification of electric field strength in the insulation region next to the conductor and metallic screen, which can occur due to the stranded structure of the conductor and the metallic screen and the presence of sharp edges on these metallic surfaces [4].

The semiconductive material, which shares a base composition similar to the insulation, plays a crucial role in this context. During the thermal cycling process, the compatibility of material properties between the semiconductive layer and the insulation minimizes the likelihood of gap formation between these layers. Any gap between the conductor and the semiconductive layer poses no danger, as both the semiconductive layer and the conductor maintain the same voltage, thus ensuring a close to zero electric field in these gaps, eliminating the possibility of partial discharge initiation.

This paper examines the application of semiconductive screening to the windings of a medium-voltage dry-type transformer. In contrast to the approaches reported in [5], [6], which employ separate XLPE-insulated cables for winding construction, the proposed method applies semiconductive screens to the entire winding structure, encompassing both the conductors and the cast-resin insulation. Although reducing air gaps through winding encapsulation can contribute to size reduction in dry-type transformers in general, this effect becomes particularly pronounced in medium-frequency transformers (MFTs). MFTs, which are key components in solid-state transformer (SST) systems, are inherently designed for compact magnetic structures. Their achievable size, however, is primarily limited by insulation constraints and thermal management considerations [7]. Dry-type MFTs offer a more straightforward and less complex alternative compared to oil-insulated MFTs. Grid-connected MFTs must withstand voltage tests, such as acceptance criteria of IEC 60076-3 [8] and IEC 60076-11 [9], regarding their types. Considering that the larger gaps cancel the main advantage of a compact SST, this paper presents a novel technique, semiconductive screening, which helps reduce the dry-type MFTs' overall size. Encapsulating the windings of a dry-type transformer also offers additional benefits, such as enhancing safety and mitigating electromagnetic interference (EMI) issues.

To tackle stray losses in medium-frequency SST applications, semiconductive screening offers a practical and effective solution, particularly in dry-type transformer designs. In oil-immersed transformers, a metallic tank naturally contains the electric field and enables termination grading via bushings. However, in dry-type transformers, the absence of such an enclosure allows the electric field to extend beyond the epoxy insulation, increasing the risk of surface discharge.

The proposed semiconductive screen serves a similar field-containment function, but with the added advantage of significantly reduced eddy current losses. Unlike metallic tanks, the semiconductive screen have limited conductivity, which minimizes the formation of eddy currents even at higher switching frequencies. Furthermore, the screen's minimal thickness further suppresses the eddy current generation. These combined properties — low conductivity and small thickness — ensure that any induced currents are weak and contribute negligibly to overall stray losses. As a result, semiconductive screening provides a compact and efficient means of controlling electric field boundaries while mitigating frequency-related losses in MFTs [10], [11].

Field grading and insulation design in SST applications are the subject of several studies [12], [13], [14], [15], [16], [17], [18]. Ref. [12] details the development and testing of two MFT prototypes for use in a three-phase Dual-Active Bridge (DAB3) DC-DC converter system. These transformers are designed to connect offshore wind farms to medium-voltage grids. The first prototype (MFT 1) required additional inductors to achieve the needed series inductance. The second prototype (MFT 2) integrated this inductance within the same core using a stacked winding configuration, eliminating the need for extra inductors. MFT 2 also featured high-voltage secondary windings insulated with semiconductive and cast resin materials, ensuring compatibility with ±25 kV medium-voltage applications.

Ref. [13] focuses on the electrical shielding of medium-voltage, medium-frequency transformers subjected to high dv/dt PWM voltages. It investigates the distribution of electric fields in the insulation, at the surface, and in the air for a specific MV/MF transformer. The study emphasizes the design of an effective shield to reduce the electric field without increasing losses. The shielding strategies employ semiconductive and resistive materials to manage the insulation challenges posed by high voltage and frequency applications, ensuring better performance and reliability of the transformers. Ref. [14] addresses the insulation design for high-frequency transformers in medium-voltage, air-cooled, silicon carbide (SiC)-enabled solid-state transformers. It proposes an insulation system integrating polymer and inorganic materials to balance high dielectric strength and thermal conductivity. This system, designed to be partial-discharge-free, demonstrates an insulation level of ±95kV and an effective thermal conductivity approximately 2-3 times higher than similar polymer materials, making it suitable for high-voltage and high-frequency applications. In [15], the authors present a study on the internal electric field shielding structure for high-voltage windings in medium-voltage, high-frequency transformers. They introduce a shielding layer incorporating low resistivity semiconductive (LSC) material and copper foil to optimize electric field distribution and enhance insulation reliability. This approach aims to reduce the peak internal electric field, thereby lowering the risk of partial discharge, and is validated with a prototype transformer that successfully passes insulation tests.

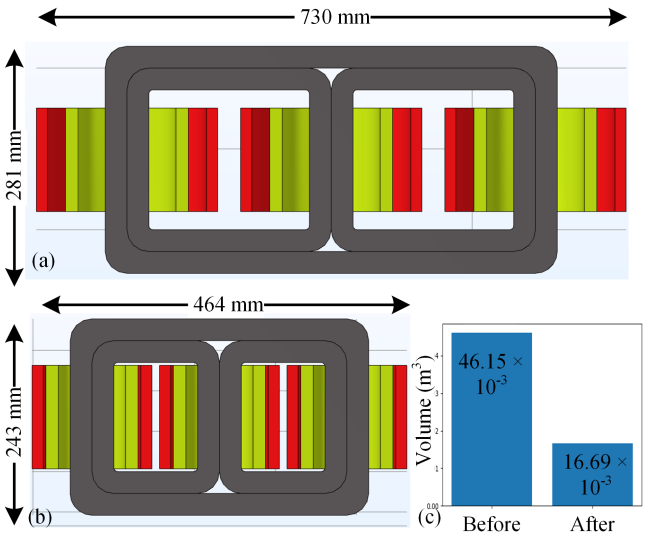

FIGURE 1. The impact of proposed method: (a) The dimensions of a 50 kW, 1 kHz MFT before applying the proposed method; (b) Similar transformer after applying the proposed method. The transformer's dimensions shrink due to smaller gaps (clearances) are needed; (c) The comparison between the overall volume of two transformers.

The subject of [16] is an improved high-voltage winding internal shielding structure for medium-voltage high-frequency transformers, focusing on reducing eddy losses. It proposes a new structure using semiconductive materials and copper foil, designed to minimize eddy current losses while maintaining effective electric field shielding. Ref. [17] focuses on the design of a high-frequency transformer with medium-voltage insulation for a resonant converter in solid-state transformers. It presents an innovative approach to insulation, using semiconductive materials to enhance electric field distribution, reduce peak internal electric fields, and lower partial discharge risks. Ref. [18] presents a planar structure high-frequency transformer design for medium-voltage applications, focusing on insulation and shielding techniques. It utilizes modular PCB boards for high-voltage side windings, where a coated semiconductive shielding layer confines the high electric field within the PCB insulation.

While previous studies have explored various field grading techniques and shielding strategies in medium-frequency transformer designs, many have focused either on planar insulation layouts or cable-based windings. However, comprehensive methods that integrate semiconductive screening directly within the epoxy-based winding encapsulation for dry-type medium-voltage transformers are lacking. The present paper builds upon established principles from HV/EHV cable technology and adapts them to transformer windings into medium-frequency solid-state applications, with the aim of improving insulation compactness and PD performance without compromising thermal dissipation or mechanical integrity.

The main contributions of the present study are as follows:

- A novel implementation of semiconductive screening for encapsulated windings in medium-voltage, medium-frequency dry-type transformers,

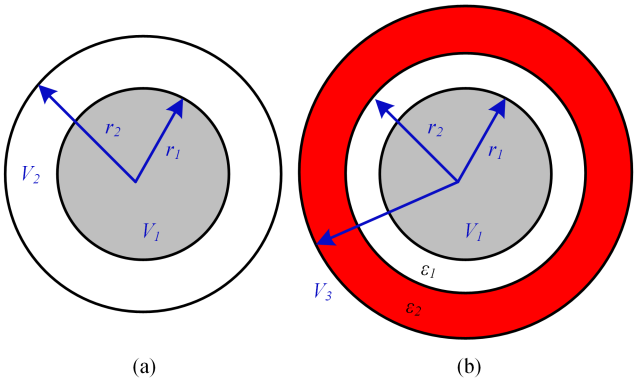

FIGURE 2. (a) Two concentric cylinders representing the windings, (b) gaps filled with different materials.

- Analytical and FEM-based modeling of electric field distribution considering mixed air-epoxy insulation media,
- A detailed design and fabrication method for stress cone-based field grading, compatible with the proposed screening technique,
- Experimental verification via partial discharge measurements demonstrates a significant PD reduction from 46.1 pC to 2.2 pC, validating the effectiveness of the proposed approach.

Fig. 1 shows the impact of applying the proposed method on the dimensions and overall volume of a 50 kW, 1 kHz MFT for green hydrogen production. Applying the proposed method results in smaller transformer and lesser environmental footprints and cost.

The rest of the present paper is organized as follows: The electric field calculation is detailed in Section II. Section III conducts the partial discharge and surface flashover in transformers. Section IV explains the field grading methods and describes the proposed approach. FEM simulation is provided in Section V, and in Section VI, experimental results are detailed. Finally, Section VII concludes the paper.

II. THE ELECTRIC FIELD IN A DRY-TYPE TRANSFORMER

This section first introduces an analytically tractable electric-field model to establish baseline radial stress levels in dry-type transformer insulation. The limitations of this idealized formulation are then explicitly addressed by considering local electric-field enhancement effects arising from practical geometrical irregularities.

The windings of a dry-type transformer can be assumed as cylinders to avoid complexity. While actual transformer windings can be rectangular in shape, the cylindrical approximation used in this study provides a simplified yet sufficiently accurate representation for analytical calculation of radial electric fields. This assumption is common in preliminary insulation analysis and enables closed-form expressions that offer intuitive insights. The electric field between the cylinders shown in Fig. 2(a) can be derived as follows:

$$E = \frac{V_1 - V_2}{r \ln \frac{r_2}{r_1}} \tag{1}$$

where V_1 and V_2 are the voltage of the inner and outer cylinders, respectively, and r_1 and r_2 are the radiuses of the cylinders. The maximum electric field, E_{max}, can be calculated as follows:

$$E_{\max} = \frac{V_1 - V_2}{r_1 \ln \frac{r_2}{r_1}} \tag{2}$$

However, the gap between windings is usually filled by different materials, such as epoxy resin and air, as shown in Fig. 2(b). Thus (1) is rewritten as follows:

$$E_i = \frac{V_1 - V_3}{r\varepsilon_i \left[\frac{1}{\varepsilon_1} \ln \frac{r_2}{r_1} + \frac{1}{\varepsilon_2} \ln \frac{r_3}{r_2}\right]}, i = 1, 2 \tag{3}$$

where ε is the relative permittivity. In a typical transformer, the low-voltage (LV) winding is placed near the core, and the high-voltage (HV) winding is placed over the LV winding. Each winding is covered with epoxy resin from both the inner and outer sides. Therefore, the problem is to calculate the electric field in the gaps and inside the epoxy resins, as shown in Fig. 3. Therefore, the field calculation problem for the LV-Core gape is as follows:

$$E_i = \frac{0 - V_{LV}}{r\varepsilon_i \left[\frac{1}{\varepsilon_0} \ln \frac{r_{LVepoxy\_in}}{r_{core}} + \frac{1}{\varepsilon_{epoxy}} \ln \frac{r_{LV\_in}}{r_{LVepoxy\_in}}\right]} \tag{4}$$

where V_{LV} is the voltage of LV winding, $r_{LVepoxy\_in}$ is the inner radius of the LV epoxy, r_{core} is the radius of core, r_{LV_in} is the inner radius of the LV winding, ε_0 is the permittivity of air, and ε_{epoxy} is the permittivity of epoxy resin. Note that the core is grounded; thus, its voltage is zero. Similarly, the electric field in the HV-LV gap can be calculated as follows:

$$E_i = \frac{V_{LV} - V_{HV}}{r\varepsilon_i \left[\begin{array}{l} \frac{1}{\varepsilon_{epoxy}} \ln \frac{r_{LVepoxy\_out}}{r_{LV\_out}} + \frac{1}{\varepsilon_0} \ln \frac{r_{HVepoxy\_in}}{r_{LVepoxy\_out}} \\ + \frac{1}{\varepsilon_{epoxy}} \ln \frac{r_{HV\_in}}{r_{HVepoxy\_in}} \end{array}\right]} \tag{5}$$

where V_{HV} is the voltage of HV winding, r_{LV_out} is the outer radius of the LV winding, $r_{HVepoxy\_in}$ is the inner radius of HV epoxy, and r_{HV_in} is the inner radius of HV winding. Therefore, the LV-Core and HV-LV gaps can be calculated from (4) and (5), respectively.

The derived field expression provides an estimate of the maximum radial field stress between conductors, which is directly related to the onset of partial discharges in solid insulation. While the above equations provide insight into the radial electric field in idealized concentric geometries, practical transformer windings exhibit more complex field behavior. Local electric field enhancements often occur due to geometric discontinuities such as bolt protrusions, casting seams, and surface roughness. As illustrated in Fig. 4, even simple features like a semi-cylindrical or semi-spherical

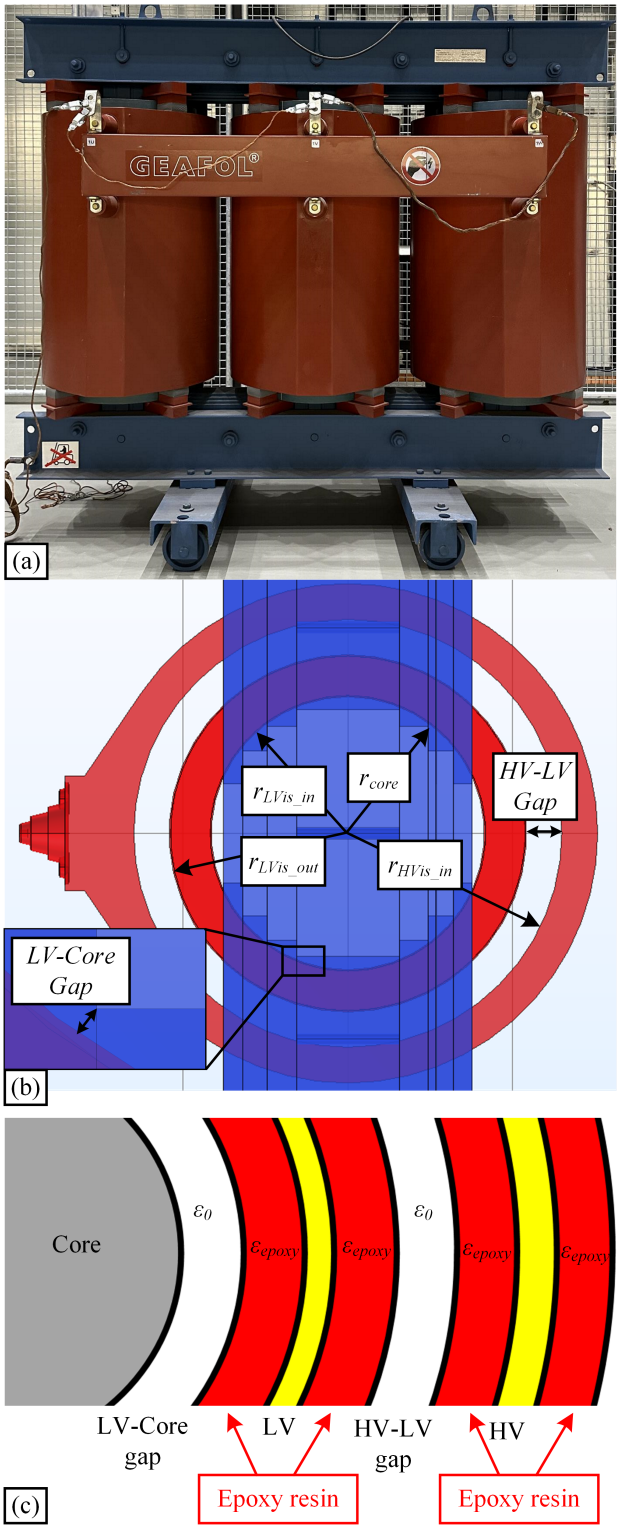

FIGURE 3. Structural overview and field configuration of a dry-type medium-voltage transformer. (a) Photograph of a three-phase cast-resin transformer, (b) cross-sectional schematic of winding geometry and gap definitions, highlighting critical insulation paths between core, low-voltage (LV), and high-voltage (HV) windings, (c) radial electric field configuration and material composition, including air gaps and epoxy-encapsulated winding sections. The labelled parameters correspond to those listed in Table 1 and are used in the analytical and FEM models.

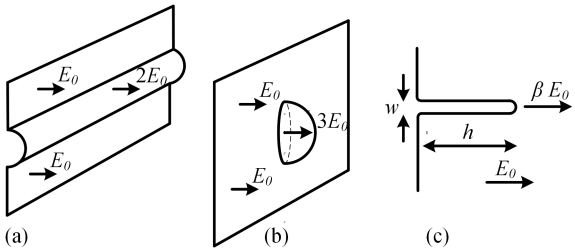

FIGURE 4. Electric field enhancement due to geometrical protrusions and surface irregularities: (a) A semi-cylindrical seam or welding joint doubles the local electric field to approximately $2E_0$, (b) a semi-spherical feature, such as a bolt head or droplet, can triple the field to $3E_0$, (c) micro-scale field enhancement at sharp tips or protrusions, where the local field is amplified by a factor of β, defined by geometry as $\beta \approx 2+h/(w/2)$. These effects demonstrate how small-scale features can significantly increase the risk of partial discharge and surface flashover, even under moderate background field conditions.

bump can increase the local field intensity by a factor of 2 to 3. Micro-protrusions can produce even greater amplification, with field enhancement factors β exceeding 40 in extreme cases. These localized effects can push the electric field beyond 1.5 MV/mm, even when the average field remains below 40 kV/mm [19].

Sharp edges, common features in transformers particularly within their cores, can enhance the electric field considerably (Fig. 5). The electric field intensity around these sharp edges can be determined using the method of conformal transformation. This approach provides a mathematical framework for analyzing electric field dynamics in areas with sharp edges [20]. However, with the advancements in numerical methods and Finite Element Method (FEM) simulations, it has become more advantageous to employ FEM for calculating non-uniform electric fields. In this paper, FEM simulations are utilized wherever necessary to enhance the precision and efficacy of electric field calculations.

Thermal considerations determine the LV-Core gap if the LV voltage is too low. However, the HV-LV gap must be designed to satisfy insulation coordination and thermal considerations. Adding more thickness to the epoxy resin is not a good practice since it decreases the gap and causes less heat transfer. The electric field in the air gap is stronger than the same parameter inside an isolation material, which has higher relative permittivity. Let material 1 be the epoxy resin that is used to build the winding insulation, and material 2 is air. The homogenous electric field is defined as follows:

$$E = \frac{V}{d} \tag{6}$$

where V and d are the applied voltage and distance, respectively. An adequate minimum air gap must be considered to keep the electric field below a certain level. Let us assume E_{PD} is the maximum acceptable electric field strength in the air to avoid partial discharge (PD). Then, the minimum size of

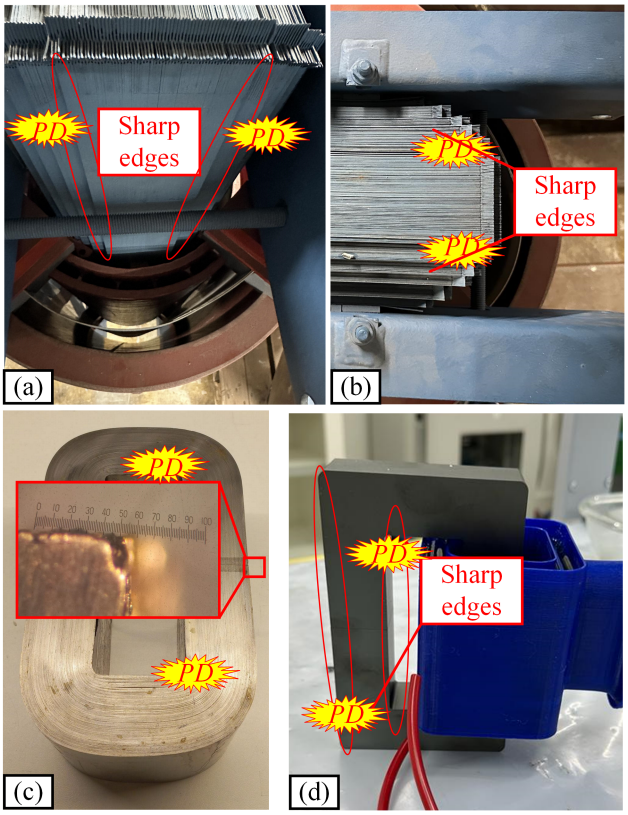

FIGURE 5. Sharp edges in different magnetic cores: (a) and (b) electrical steel 50 Hz core, (c) amorphous core, and (d) ferrite core.

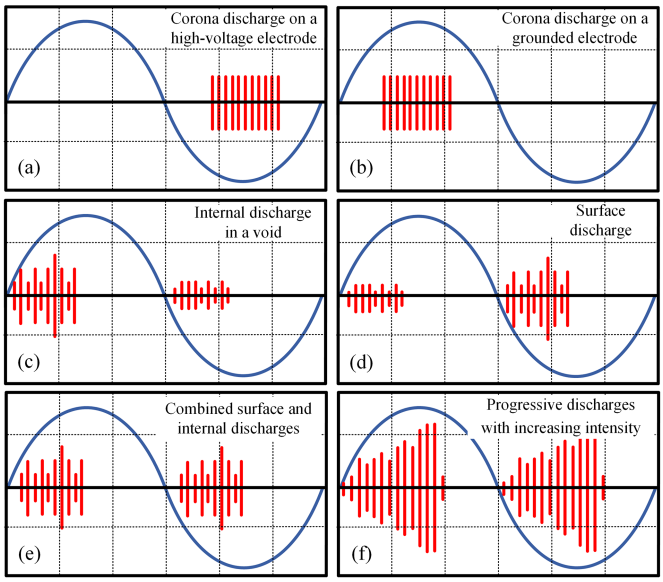

FIGURE 6. Oscilloscope response patterns of different types of partial discharge (PD). The blue waveform shows the phase of the applied AC voltage, while the red pulses indicate detected PD events. These phase-resolved patterns are commonly used to identify and classify the source of discharges: (a) Corona discharge on a high-voltage electrode, (b) corona discharge on a grounded electrode, (c) internal discharge in a void, (d) surface discharge, (e) combined surface and internal discharges, (f) progressive discharges with increasing intensity. These patterns are used to interpret PD test results and assess insulation behavior under different conditions.

the air gap can be calculated as follows:

$$d_{air} = \frac{V - \frac{E_{PD}}{\varepsilon_r} \times t_{is}}{E_{PD}} \tag{7}$$

where V is the applied voltage, ε_r is the relative permittivity of the insulation (epoxy resin), and t_{is} is the thickness of the insulation.

While the above equations provide insight into the radial electric field in idealized concentric geometries, they intentionally represent a lower-bound estimate of electric-field stress. In practical transformer windings, local geometric discontinuities introduce strong field non-uniformities that dominate partial-discharge inception. These analytical considerations motivate the need to control both global and local electric-field stress, which directly governs partial discharge inception and surface flashover behavior discussed in the following section.

III. PARTIAL DISCHARGES AND SURFACE FLASHOVER IN TRANSFORMERS

As shown in Section II, even moderate average electric-field levels can result in critical local overstress due to geometrical irregularities, making partial discharge and surface flashover the dominant insulation-limiting mechanisms in dry-type transformers.

Understanding and controlling partial discharges and surface flashover is essential, as these phenomena determine the electrical clearance requirements in transformer design. Reducing their occurrence enables more compact insulation design. Partial discharges (PDs) and surface flashover events are often the limiting factors in determining insulation clearances in dry-type transformers. The required distances between conductors, or between conductors and grounded components, are primarily dictated by the electric field intensity that initiates these effects. Therefore, mitigation of PDs and surface discharges enables more compact insulation design, which directly contributes to transformer miniaturization.

A. PARTIAL DISCHARGES

Partial Discharge (PD) in transformers is a critical phenomenon that refers to localized electrical discharges within the insulation system of the high-voltage electrical equipment [21], [22], [23], [24], [25], [26]. These discharges can happen when the insulation is weak or damaged, leading to gradual deterioration. The importance of mitigating PDs lies in their potential to cause insulation failure, resulting in costly downtime, hazardous working conditions, and reduced equipment lifespan. Early detection and management of PDs are crucial for ensuring the reliability and safety of power systems [27]. Analyzing the PD requires knowledge about PD patterns. Various patterns of PD are summarized in Fig. 6 [21], [28], [29].

The primary cause of partial discharge (PD) in transformers is the presence of sharp edges, particularly around the core. These edges act as stress concentrators, significantly enhancing local electric fields and initiating PD. This phenomenon is most noticeable when geometric irregularities, like those of the core, disrupt the uniformity of the electric field distribution. In 50 Hz transformers, using electrical steel sheets often results in sharp edges, which can be a significant source of PD difficulties. On the other hand, in medium-frequency or high-frequency transformers, the ferrite cores and cores made from amorphous strips tend to have sharp edges, similarly giving rise to challenges associated with PD (Fig. 5).

An additional challenge in medium-frequency or high-frequency transformers arises from the necessity of using litz wires to mitigate copper loss at higher frequencies. However, this approach introduces a new problem: PD occurring between two adjacent litz wires due to the presence of air bubbles trapped in litz wire strands. Moreover, due to the complex shape of the litz wire, the impregnating medium, such as the epoxy resin, may not stick very well to each other, and even during thermal cycles, different thermal expansion coefficients between the two might cause separation and formation of cavities which causes PDs and long term aging and failure. As a solution, [15] proposes using internal electric field shielding, which has effectively mitigated the possibility of the formation of PD.

Besides the factors mentioned above, other elements also influence the presence of PD in transformers. Among these, the presence of air bubbles in the epoxy resin during the casting process is particularly critical. A meticulous casting procedure is essential to guarantee the absence of air bubbles within the epoxy, involving precise step-by-step pre-heating, pre-degassing, mixing, casting, degassing, curing, and cooling, each of which must be conducted with precision to minimize the risk of PD.

B. SURFACE FLASHOVER

Surface flashover occurs along the improperly designed termination. Applying a coating to the conductors and increasing the distance between them does not necessarily mitigate all risks associated with the insulation system of a dry-type transformer. Surface discharges occur when the applied voltage surpasses a certain threshold, leading to an intensified electric field caused by these initial discharges. This intensified field becomes adequate to initiate the propagation of discharge. A series of such discharges eventually triggers a surface flashover along the entire length of a winding, occurring at lower voltage levels compared to other types of electrical breakdowns [30], [31]. Therefore, proper termination is necessary to avoid flashover. Fig. 7 illustrates a surface flashover incident, where, due to improper termination, a flashover occurred over a considerable distance from the high voltage point to the grounded core.

Understanding the conditions under which PDs and flashovers initiate helps define the motivation for implementing field control techniques, such as semiconductive screening and stress cone shaping, which are detailed in the subsequent sections.

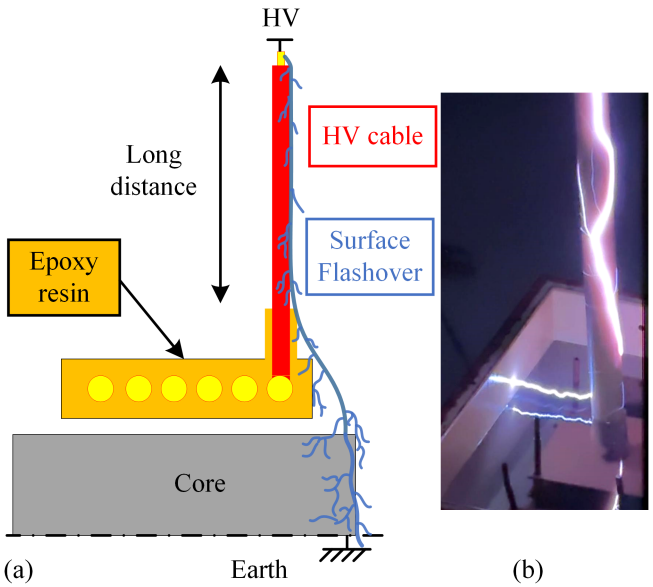

FIGURE 7. (a) Surface flashover through long distance between HV and the core, (b) the surface flashover captured in the lab over long distance during a test.

IV. FIELD GRADING METHODS

Although electrode-based field grading slightly increases the volume at the winding terminations, it enables a significant overall reduction in insulation distances by mitigating electric field stress, which in turn supports transformer miniaturization.

Several methods are available to enhance electric field distribution, including electrode grading, epsilon grading, condenser grading, and resistive grading, as depicted in Fig. 8 [32], [33]. Among these, electrode grading is often preferred due to its numerous advantages. This method enables precise control over electric field distribution by shaping the electrodes to achieve a more uniform field. This uniformity reduces peak electric field strength and lessens the risk of dielectric breakdown, particularly at points of natural field intensification, such as sharp corners or edges. Electrode grading's efficiency also lies in its minimal material requirements, contrasting with epsilon grading, which depends on dielectrics with specific permittivity, or resistive and condenser grading that requires additional components to act as resistance or capacitance. Simply reshaping existing electrode designs is material-efficient and versatile, applicable across various components and systems, from high-voltage transmission lines to transformers and capacitors. This versatility often translates into cost-effectiveness, avoiding the expense of adding extra components. In addition, the manufacturing costs are generally lower, and the likelihood of defects is reduced since the process involves modifying existing designs rather than introducing new elements. Graded electrodes, designed appropriately, are less likely to degrade compared to resistive

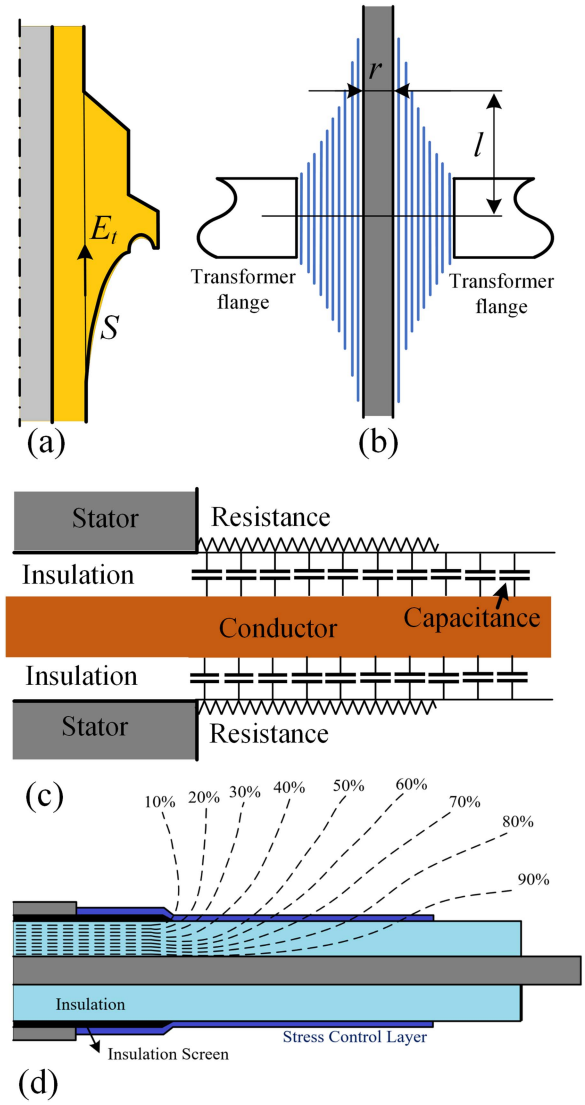

FIGURE 8. **Field grading methods in practice [30]: (a) Electrode grading using stress cone, (b) condenser bushing using floating foils (the length of the foils is graded in such a way that the capacitances between foils are constant). These layers are not directly connected to ground or high voltage but achieve a voltage gradient passively through capacitive coupling, (c) resistive grading in the stator of a HV machine under AC conditions, where *R* represents dielectric loss and *C* the capacitive coupling between conductive parts. This model reflects the dominance of displacement current at operating frequencies and avoids overestimating leakage current, and (d) epsilon grading in a cable termination [31].**

or capacitive elements, leading to extended service life and reduced maintenance. Importantly, electrode grading focuses on design rather than incorporating dissipative components, contributing to more energy-efficient operations. Therefore, this study opts for an electrode grading method based on a stress cone for further explanation.

Bushings are crucial for insulating and supporting high-voltage conductors. However, due to design complexities and material properties, they face notable limitations in medium-frequency applications. A vital issue is capacitance and impedance matching. Transformer bushings inherently have capacitance, which at higher frequencies causes reactance, disrupting impedance matching connected circuits. This issue becomes more severe as frequency increases, leading to inefficiencies and signal distortions, necessitating careful design considerations for effective medium-frequency performance.

Material limitations further limit the transformer bushings for higher frequencies. Standard materials like porcelain or resin-impregnated paper may not effectively withstand the stress of higher frequencies. Their electrical properties can change at such frequencies, leading to decreased reliability and a shorter lifespan. Moreover, bushings are subject to Frequency-Dependent Loss Factors, where insulation materials' loss factors increase at higher frequencies, causing inefficiencies and overheating risks. This necessitates choosing materials that can endure the demands of medium-frequency applications.

Additionally, manufacturing tolerances become important at higher frequencies. The production process must achieve acceptable tolerances, as even minor imperfections significantly impact performance at these frequencies. This precision requirement heightens both the complexity and cost of producing bushings for medium-frequency applications, leading to a substantial challenge in design and manufacturing. The present study employs electrode field grading as the preferred method for addressing the electric field distribution challenges in transformer bushings, particularly in medium-frequency environments, due to its efficiency, material economy, and adaptability across various applications.

A. ELECTRODE FIELD GRADING USING STRESS CONE

The primary purpose of field grading is to prevent excessive electric field strengths that can lead to breakdowns or failures in insulation materials. In high-voltage systems, sharp edges or points can create areas of high electric field strength, which can cause partial discharges or even complete insulation breakdown [21], [32].

Field grading is often achieved using materials with specific electrical properties or by shaping the conductors and insulating materials to distribute the electric field more evenly. For example, grading rings, made of conductive or semiconductive materials, are often placed around high-voltage equipment to smooth out the electric field. Proper design for field grading involves understanding the electric field distribution under various conditions, selecting appropriate materials, and shaping components to minimize areas of high electric field concentration. The primary challenge encountered in previous attempts to employ semiconductive screening for the encapsulation of MFT windings lies in the effective management of the electric field. When a semiconductive shield is positioned around a high-voltage conductor coated with epoxy resin, it neutralizes the electric field in the surrounding air. Nevertheless, a significant concern arises at the shield's end, where the electric field may intensify to hazardous levels, potentially leading to partial discharge (PD) or, in severe cases, electrical breakdown. However, as shown in Fig. 9, proper termination can mitigate this challenge significantly.

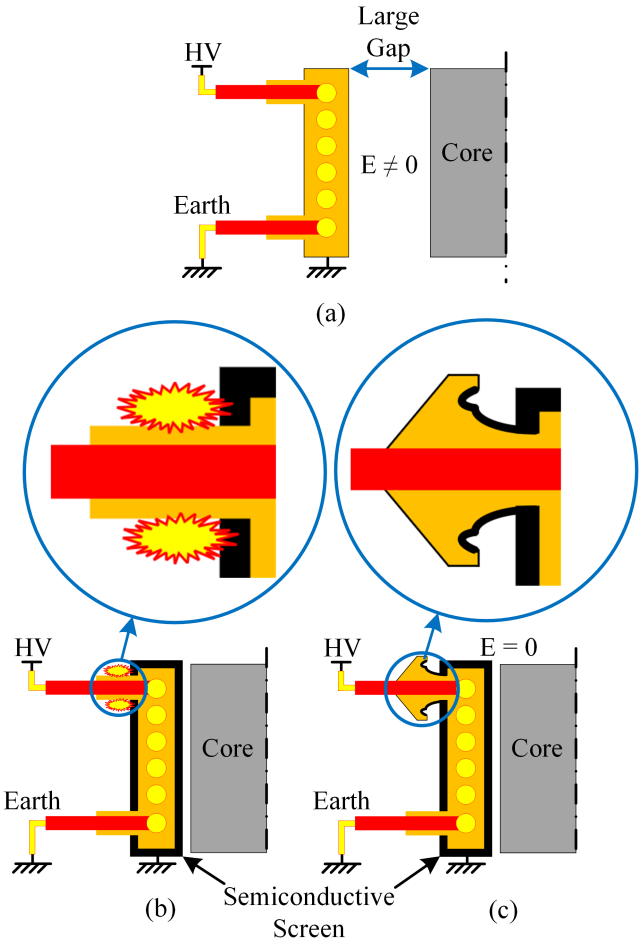

FIGURE 9. Conceptual comparison of electric field behavior at transformer winding terminations: (a) No screening — large gap and uncontrolled electric field (E ≠ 0) between winding and core, (b) the high electric field concentration at the edge of the semiconductive screen termination without proper grading, leading to discharge risk, (c) electric field mitigation using a stress cone structure. The field is smoothly graded, reducing the risk of breakdown and enabling more compact insulation design. Although the air gap increases the local electric field strength due to its lower permittivity, it is intentionally included to enable cooling and heat dissipation between the HV and LV windings. The field grading design ensures that PD-free operation is still maintained.

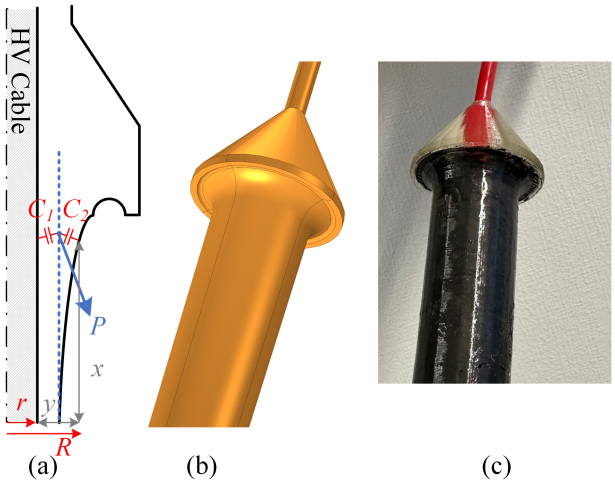

FIGURE 10. (a) The cross-sectional schematic of stress cone, (b) the 3D view of the stress cone, (c) the stress cone used in experiments (the semiconductive paint is applied).

A stress cone in a cable terminal is an excellent example of electrode grading, as shown in Fig. 10. The cable field is gradually reduced to prevent field concentrations and to create an even potential distribution over the external insulator. The shape of the stress cone is optimized by keeping the potential gradient along the interface $\Delta P/\Delta x$ constant. The curve can be designed as follows [21]:

$$x = \frac{V}{E_t}\left(1 - \frac{\ln(R/r)}{\ln(y/r)}\right) \tag{8}$$

where E_t is the tangential field, and R and r are shown in Fig. 10. E_t is selected to maintain a maximum of 0.5 kV/mm at nominal voltage [21]. Mechanically, R must remain within the boundaries of the epoxy casting and available space. An initial approximation of $2r < R < 3r$ is used in practice, and then refined using FEM simulations to verify field distribution and ensure safe operation under medium-frequency stress conditions. The stress cone for field grading is applied for the field treatment at the end of the semiconductive screen in the present study.

The stress cone geometry was selected to ensure a smooth transition of the electric field from the high-voltage winding to the grounded surrounding structure. The cone angle and electrode extension length were chosen based on iterative FEM simulations to reduce field peaks and maintain electric field strength below 0.5 kV/mm in the surrounding air and interface regions. The dimensions also satisfy minimum clearance requirements outlined in IEC 60076-11 [9]. This configuration ensures effective field grading while maintaining compactness suitable for dry-type MFT designs.

The combination of the upper stress cone and the surrounding field control ring increases the effective creepage distance and provides smoother field gradients. This integrated approach enables compliance with IEC 60076-11 [9] insulation requirements within a compact geometry. Although stress cones are traditionally used in MV cable terminations, their application in MFTs addresses similar field enhancement issues at winding terminations, particularly in compact dry-type designs where sharp edges and limited air clearances increase the risk of partial discharges.

B. SEMICONDUCTIVE SCREENING

To reduce the electric field inside the gaps, semiconductive screening is performed to provide a semiconductive surface around the windings. This surface encapsulates the electric field; therefore, the electric field in the gap is zero (E_{gap} = 0 kV/mm). Semiconductive materials are preferred over conductive shields to enhance the system's efficiency. This choice is crucial to mitigate additional losses of the conductive shield.

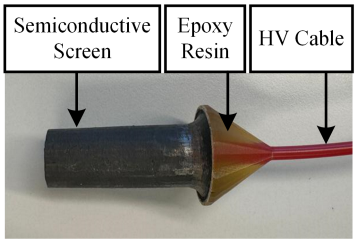

FIGURE 11. Semiconductive screen sticks to the epoxy resin.

TABLE 2. Characteristics of Semiconductive Compound

Base compound	Conductive filler	Ratio	Conductivity
Butyl Acetate, Ethyl Acetate, Neopentyl Glycol	Graphite powder	85:15	5.23×10^{-6} S/m (at 20C, for typical thickness = 100 µm)*

* A fine-brush application method was adopted to deposit the semiconductive layer with a controlled minimum thickness of about 100 µm. Experimental evaluation showed that this thickness was sufficient to suppress partial discharges without introducing significant local loss mechanisms.

The presence of eddy currents induced by the magnetic field can lead to unwanted extra loss and heat generation, which can be effectively addressed using semiconductive materials. The stickiness of the semiconductive screen to the epoxy resin is essential, as any looseness or the presence of air bubbles can result in localized areas of high electric field strength. Strict adherence ensures uniform distribution of the electric field and prevents potential complications from inconsistencies in the bonding.

The composition of the semiconductive compound includes two parts. Part one is a blend of Butyl Acetate ($CH_3CO_2(CH_2)_3CH_3$), Ethyl Acetate($C_4H_8O_2$), and Neopentyl Glycol ($C_5H_{12}O_2$), which is commercially available and used for different purposes such as adhesives and coatings. Part two is graphite powder to provide conductivity. The mixture is 85:15 weight-wise. This balanced mixture ensures optimal conductivity and stability. The semiconductive compound exhibits excellent adhesion to various epoxy resins and has robust conductivity. This versatility and high performance make it an ideal choice for applications requiring reliable electrical conductivity and strong bonding properties. Fig. 11 shows the semiconductive screen, and Table 2 summarizes its characteristics. The compound is commercially available in adhesive and nail polish formulations, and in this study, it was applied manually using a small brush to ensure uniform coverage and strong adhesion to the epoxy resin.

V. FEM SIMULATIONS AND MODEL DEFINITION

The finite-element simulations presented in this section were performed using COMSOL Multiphysics to reproduce the experimental stress cone configuration under realistic insulation and boundary conditions. A two-dimensional axisymmetric

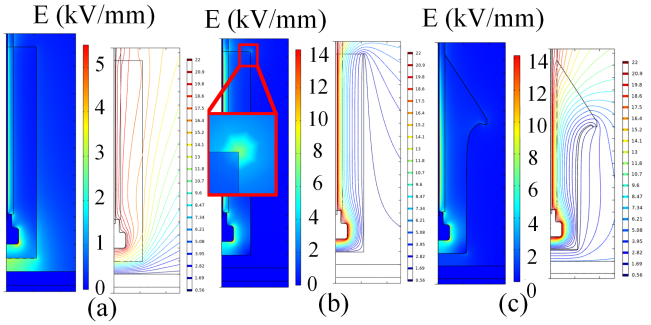

FIGURE 12. Electric field simulation results at the stress cone termination (a) without semiconductive shield, (b) with semiconductive shield but no proper termination, and (c) with both semiconductive shield and optimized stress cone termination. The semiconductive layer significantly reduces the electric field concentration in the air gap and on the epoxy surface.

model was employed, which is appropriate for the rotationally symmetric geometry of the stress cone and enables accurate evaluation of electric field distribution with reduced computational complexity.

Accurately solving complex electric field calculations is important, but it is complex for field grading problems. The Finite Element Method (FEM), COMSOL Multiphysics software in the present study, is employed to examine the impact of the semiconductive screening and proper termination of the transformer. A COMSOL 2D axis-symmetrical simulation is performed in the present study to analyze the effect of semiconductive screening on field grading. The setup includes an electrode, part of a high-voltage cable encapsulated in epoxy resin. A grounded plate electrode is placed to represent the influence of a core adjacent to the high-voltage electrode. Without the semiconductive screen, the simulation reveals an alarmingly high electric field strength in the air gap between the epoxy resin and the grounded electrode.

In contrast, introducing a semiconductive screen on the cone reduces the electric field strength in this gap to nearly zero, as illustrated in Fig. 12(a) and (b). However, without proper termination, the electric field can be significantly higher on top of the epoxy resin. Proper termination can mitigate the intensity of the electric field, as depicted in Fig. 12(b) and (c). These results clearly demonstrate the optimization effect of the semiconductive shield in reducing local field enhancements at the stress cone termination.

The stress cone and screening configuration were designed to replicate real dry-type MFT insulation geometries and meet IEC 60076-11 [9] voltage test requirements. In the simulation, the inner electrode was energized at 22.75 kVrms, while the grounded plate represented the transformer core potential. The outer surface of the semiconductive screen was assigned zero potential to simulate electrical grounding. Material properties were defined as follows: the epoxy resin with a relative permittivity of 3.5 and the surrounding air with a relative permittivity of 1. These conditions replicate the actual insulation environment observed in the laboratory tests. These boundary conditions and material properties were selected to directly

correspond to the laboratory test configuration used for partial discharge measurements, ensuring consistency between numerical and experimental results.

The setup ensures a representative field distribution while remaining suitable for laboratory PD measurement. Future developments of the test campaign will include thermal cycling, long-duration PD endurance testing, and evaluation on a complete transformer system. While the present prototype focuses on epoxy cast insulation around the windings and terminations, future work may incorporate layered film insulation (e.g., polyimide) to study combined inter-turn and global field behavior.

VI. EXPERIMENTAL RESULTS

The experimental design presented in this section is intended as a focused proof-of-concept study to evaluate the effectiveness of semiconductive screening and stress cone–based field grading under controlled and repeatable conditions. The test object geometry, material selection, and voltage levels were chosen to represent critical insulation interfaces in dry-type medium-frequency transformers while remaining compatible with standardized partial discharge measurement procedures.

Although the applied test voltage follows a 50 Hz sinusoidal waveform in compliance with IEC standards, the evaluated insulation interfaces and field grading mechanisms are independent of the excitation waveform and therefore relevant as a baseline for subsequent studies under converter-driven voltage stress.

A. STRESS CONE PREPARATION

The epoxy casting process was performed in a vacuum oven under carefully controlled thermal and pressure conditions to eliminate air voids. This procedure replicates industrial casting methods and was refined in the lab over several years to ensure void-free insulation. The highest voltage for the equipment for the transformer is 17.5 kV_{rms}. Therefore, the stress cone for the field grading is designed to handle an applied test voltage of 22.75 kV_{rms} regarding IEC 60076-11 during the partial discharge measurement. The test is fulfilled if the maximum level of PD is 10 pC or less [9]. This voltage level is consistent with IEC 60076-11 requirements for dry-type transformers and corresponds to typical voltage stress conditions in medium-voltage SST applications. The minimum air clearance from the HV terminal to the grounded screen edge was 28 mm, and the creepage distance along the epoxy surface was over 50 mm.

The cone is made of a two-part epoxy resin called CY225-HY225, which is common in transformer manufacturing. The manufacturing process for the stress cone is meticulously designed and executed in the following steps:

1) *3D Printing of the Cone:* Initially, the cone is crafted using a 3D printer, utilizing Polylactic Acid (PLA) for its construction. This step ensures high accuracy in the cone's dimensions and shape.
2) *Creation of a Silicon Rubber Mold:* Utilizing the 3D printed cone, a mold is cast from silicon rubber. This mold is vital for accurately replicating the shape and dimensions of the cone in subsequent stages. The silicone mold used to shape the epoxy stress cone was fabricated using a commercially available silicone rubber compound, chosen for its mechanical flexibility and compatibility with the epoxy curing temperature.
3) *Preparation of Cable and Electrode Assembly:* The cable and electrode are carefully positioned within the silicon rubber mold. This setup is then prepared for the next step - the casting of the epoxy resin.
4) *Epoxy Resin Preparation:* The epoxy resin is accurately mixed, pre-heated, and pre-degassed using a vacuum oven. This preparation is necessary to ensure the resin's optimal flow and adhesion properties.
5) *Casting and Degassing of Epoxy Resin:* The prepared epoxy resin is then cast into the mold. Following the casting, a degassing process is employed to eliminate any trapped air bubbles, ensuring the integrity and electrical properties of the molded component.
6) *Curing of Epoxy Resin:* Once cast, the epoxy resin is heated to its curing temperature, maintained at 140°C. This step is vital for achieving the desired mechanical strength and electrical insulation properties.
7) *Mold Removal and Semiconductive Screening:* The mold is carefully removed after the resin has cured. Subsequently, the semiconductive screen is applied. This final step is pivotal in enhancing the final product's electric field grading capabilities.

Each step in this procedure is essential for achieving the desired characteristics and performance of the stress cone in its application. Fig. 13 shows details of the stress cone preparation process. To ensure consistency and eliminate internal voids, the epoxy was mixed and degassed under vacuum before casting and was subjected to additional degassing after pouring. All samples were visually inspected and tested for partial discharge activity to confirm the absence of air bubbles or void-related insulation defects. The semiconductive screen was applied after curing using a controlled brush-coating technique, ensuring uniform coverage across all samples.

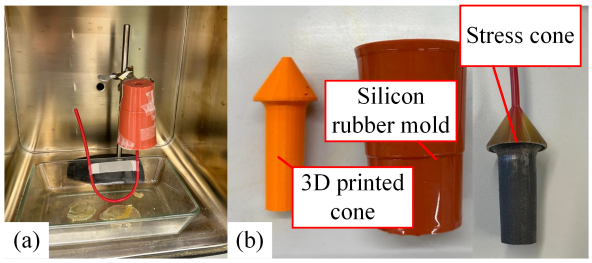

FIGURE 13. (a) The degassing procedure inside the vacuum oven, (b) the 3D printed cone, the silicon rubber mold, and the casted stress cone.

B. PARTIAL DISCHARGE MEASUREMENT FOR THE STRESS CONE

The partial discharge (PD) measurement in the present study is conducted using the criteria of IEC 60270 [34] and IEC

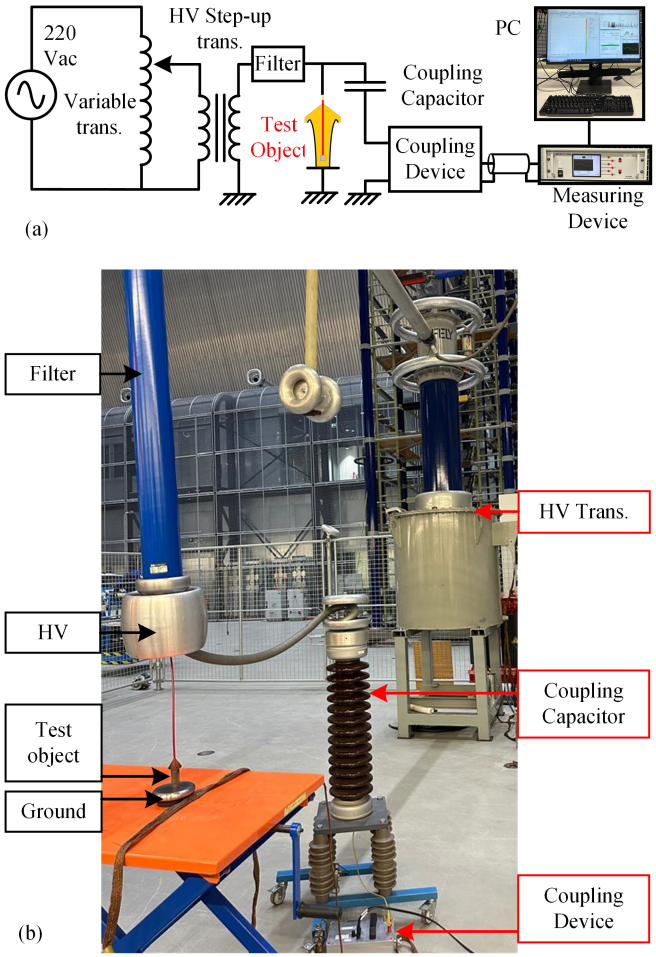

FIGURE 14. The PD measurement setup: (a) The block diagram, (b) the laboratory setup.

TABLE 3. PD Measurement Setup Characteristics

Component	Manufacturer	Type
HV step-up transformer	Haefely	TEOS 0.5/200 kV 100 kVA
Coupling capacitor	Haefely	1062 pF 100 kV
Measuring device	Hubbell	DDX-9101

60076-11 [9]. The experimental setup, illustrated in Fig. 14, consisted of six key components: an HV step-up transformer, the test object, a filter, a coupling capacitor, a coupling device, and a measuring device. The setup components are listed in Table 3. The background noise of the test setup was measured to be less than 0.8 pC, ensuring the accuracy of the PD measurements. The results of the PD measurements are presented in Fig. 15. These figures compare the PD behavior of the stress cone under two different conditions: (a) without semiconductive screening and (b) with semiconductive screening applied. The schematic diagrams represent the test setup for both cases, highlighting the addition of the semiconductive screen

TABLE 4. PD Measurement Results

	Max Applied Voltage (kV_{rms})	Max PD Level (pC)	Test Time (s)	Noise Level (pC)
No Semi. Con. Paint	17.5 kV	46.1	250	0.8
Semi. Con. Pant	25 kV	2.2	360	

in the configuration (Fig. 15(b)). The upper plots present the Partial Discharge (PD) activity over time, showing a significant reduction in PD magnitude and occurrence after applying the semiconductive screen.

The Phase Resolved Partial Discharge (PRPD) plots display the phase angle of the applied voltage (0–360°) on the horizontal axis, the PD magnitude in pico-Coulombs (pC) on the vertical axis, and the density of discharge events represented by a color bar.

In the absence of semiconductive screening, as shown in Fig. 15(a), significant PD activity is observed, with discharge events concentrated around the high-field regions near the voltage peaks. The test object acts as a floating electrode, resulting in localized field enhancements and higher PD activity, with a maximum PD magnitude exceeding 46.1 pC. A considerable number of events fall within the range of 10–40 pC.

In contrast, Fig. 15(b) demonstrates the PD performance after applying semiconductive screening to the stress cone. The screening effectively reduces the localized field concentrations, significantly lowering the overall PD activity. No discharge events exceeding 2.2 pC were recorded during the tests, reflecting a considerable improvement in insulation performance. The results indicate that the semiconductive screening ensures a more uniform electric field distribution, thus mitigating PD and enhancing the reliability of the insulation system. The observed reduction in PD levels aligns with the design goals for medium- and high-voltage insulation systems, ensuring long-term operational reliability.

The PD measurement results are summarized in Table 4. The applied voltage and test time differ between the two cases due to the presence or absence of semiconductive screening. For the configuration without semiconductive paint, the applied voltage was set considerably lower than the recommended value of 25 kV_{rms}, as significant PD activity caused the saturation of the PD detector amplifier. In contrast, after the application of the semiconductive paint, the PD activity was significantly suppressed. This allowed the test voltage to reach the recommended value (25 kV_{rms}) and extend the test time (360 s). The maximum PD level and the number of PD incidents were significantly lower, demonstrating the effectiveness of semiconductive screening in improving insulation performance.

This direct comparison highlights the effectiveness of semiconductive screening in reducing partial discharge activity and supports the practical necessity of the proposed method.

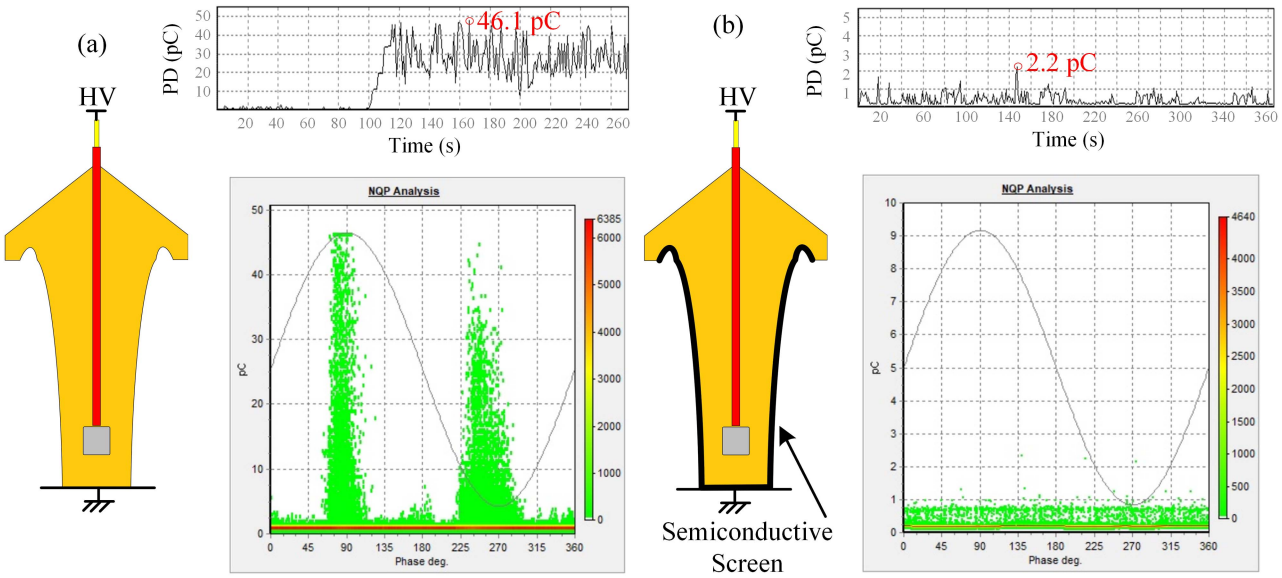

FIGURE 15. **Partial discharge (PD) measurement results for the stress cone: (a) Without semiconductive screening, showing significant PD activity and localized field enhancements, (b) with semiconductive screening, demonstrating reduced PD activity and improved electric field uniformity. The upper plots illustrate PD over time and the lower plots show the phase-resolved partial discharge (PRPD) patterns.**

While the present study focuses on short-duration partial discharge measurements under standardized 50 Hz excitation, the proposed screening and termination concept is intended for medium-frequency applications. Future experimental work will therefore include thermal cycling, long-duration PD endurance testing, and evaluation under repetitive voltage stress. In addition, implementation on a complete dry-type MFT prototype will be investigated to assess system-level performance and long-term reliability.

VII. CONCLUSION

This study presented a practical and experimentally validated approach for partial discharge (PD) mitigation in medium-voltage, medium-frequency dry-type transformers using semiconductive screening combined with stress-cone-based field grading. Drawing on established principles from high-voltage cable technology, the proposed method was adapted to epoxy-encapsulated transformer windings to enable more compact insulation design while maintaining reliable electric field control.

Analytical calculations and finite-element simulations were used to investigate electric field distribution in both idealized and non-uniform geometries, highlighting the role of geometric discontinuities in local field enhancement and PD inception. Based on these insights, a stress cone termination with integrated semiconductive screening was designed and fabricated. Experimental partial discharge measurements demonstrated a significant improvement in insulation performance, with the maximum PD magnitude reduced from 46.1 pC at 17.5 kVrms to 2.2 pC at 25 kVrms for the same encapsulated structure when semiconductive screening was applied.

All partial discharge measurements were performed under standard 50 Hz sinusoidal excitation in accordance with IEC 60270 and IEC 60076-11. Although this waveform does not replicate the high dv/dt rectangular voltages typically encountered in solid-state transformer applications, it provides a standardized and repeatable reference for insulation qualification and enables clear assessment of the effectiveness of the proposed field grading approach.

Future work will extend the present study toward more realistic operating conditions, including partial discharge and aging investigations under repetitive pulse voltages and rectangular waveforms representative of power-electronic converters. Additional developments will include long-term thermal cycling, endurance testing, and implementation of the proposed screening concept in a full-scale dry-type medium-frequency transformer to assess system-level performance and long-term reliability.

REFERENCES

[1] J. H. Harlow, *Electric Power Transformer Engineering*. New York, NY, USA: Taylor & Francis Group, 2012.
[2] P. K. Dooley, "A comparison of liquid-filled and dry-type transformers for industrial applications," *IEEE Trans. Ind. Appl.*, vol. 34, no. 1, pp. 222–226, Jan./Feb. 1998, doi: 10.1109/28.658749.
[3] R. Heinrich, S. Bonisch, D. Pommerenke, R. Jobava, and W. Kalkner, "Broadband measurement of the conductivity and the permittivity of semiconducting materials in high voltage XLPE cables," in *Proc. 8th Int. Conf. Dielectric Mater., Meas. Appl.*, 2000, pp. 212–217, doi: 10.1049/cp:20000507.
[4] B. Zhu, Z. Jia, H. Hu, X. Ouyang, and X. Wang, "Relationship between the interfacial ramped DC breakdown voltage and the morphology of the XLPE/SiR interface," *IEEE Trans. Dielectr. Electr. Insul.*, vol. 26, no. 3, pp. 689–697, Jun. 2019, doi: 10.1109/TDEI.2018.007600.
[5] M. Leijon and T. Andersson, "High and dry [Dryformer power transformer]," *IEE Rev.*, vol. 46, no. 4, pp. 9–15, 2000, doi: 10.1049/ir:20000401.

[6] Y. Gao, S. Wang, and H. Gao, "A new type of dry power transformer based on XLPE cable winding," in *Proc. Int. Conf. Elect. Mach. Syst.*, 2005, pp. 1771–1774, doi: 10.1109/ICEMS.2005.202864.

[7] Z. Li et al., "Medium-voltage solid-state transformer design for large-scale H2 electrolyzers," *IEEE Open J. Power Electron.*, vol. 5, pp. 936–955, 2024, doi: 10.1109/OJPEL.2024.3414151.

[8] *Power Transformers - Part 3: Insulation Levels, Dielectric Tests and External Clearances in Air*, Standard IEC 60076-3, International Electrotechnical Commission, Geneva, Switzerland, 2018.

[9] *Power Transformers - Part 11: Dry-Type Transformers*, Standard IEC 60076-11, International Electrotechnical Commission, Geneva, Switzerland, 2018.

[10] T. Tang, J. A. Ferreira, S. Mao, W. Wang, and M. G. Niasar, "Design of a medium frequency transformer with high insulation level for dual active bridge DC-DC converter," in *Proc. 10th Int. Conf. Power Electron. ECCE Asia*, 2019, pp. 1–8, doi: 10.23919/ICPE2019-ECCEAsia42246.2019.8797083.

[11] S. Shah and M. G. Niasar, "The effect of bending fatigue on the breakdown strength of polymer-insulated conductors," in *Proc. 11th Int. Conf. Power Insulated Cable*, 2023.

[12] M. Kaymak, R. W. D. Doncker, and T. Jimichi, "Design and verification of a medium-frequency transformer in a three-phase dual-active bridge DC-DC converter for medium-voltage grid connection of offshore wind farms," in *Proc. IEEE Appl. Power Electron. Conf. Expo.*, 2020, pp. 2694–2701, doi: 10.1109/APEC39645.2020.9124482.

[13] T. Guillod, F. Krismer, and J. W. Kolar, "Electrical shielding of MV/MF transformers subjected to high dv/dt PWM voltages," in *Proc. IEEE Appl. Power Electron. Conf. Expo.*, 2017, pp. 2502–2510, doi: 10.1109/APEC.2017.7931050.

[14] Q. Chen, R. Raju, D. Dong, and M. Agamy, "High frequency transformer insulation in medium voltage SiC enabled air-cooled solid-state transformers," in *Proc. IEEE Energy Convers. Congr. Expo.*, 2018, pp. 2436–2443, doi: 10.1109/ECCE.2018.8557849.

[15] R. Lu, J. Yu, C. Li, C. Li, W. Li, and X. He, "High voltage winding internal electric field shielding structure for medium voltage high frequency transformers," *IEEE Trans. Power Electron.*, vol. 37, no. 10, pp. 11469–11474, Oct. 2022, doi: 10.1109/TPEL.2022.3169019.

[16] R. Lu, C. Li, J. Yu, Y. Yao, W. Li, and X. He, "An improved high voltage winding internal shielding structure with lower eddy loss for medium voltage high-frequency transformer," *IEEE Trans. Power Electron.*, vol. 38, no. 12, pp. 15115–15120, Dec. 2023, doi: 10.1109/TPEL.2023.3313960.

[17] Z. Li, E. Hsieh, Q. Li, and F. C. Lee, "High-frequency transformer design with medium-voltage insulation for resonant converter in solid-state transformer," *IEEE Trans. Power Electron.*, vol. 38, no. 8, pp. 9917–9932, Aug. 2023, doi: 10.1109/TPEL.2023.3279030.

[18] R. Wang, Z. Shen, C. Zhang, B. Zhang, and P. Barbosa, "Planar structure high-frequency transformer design for medium voltage applications," in *Proc. IEEE Energy Convers. Congr. Expo.*, 2022, pp. 1–6, doi: 10.1109/ECCE50734.2022.9947429.

[19] R. V. Latham, *High Voltage Vacuum Insulation : The Physical Basis*. New York, NY, USA: Academic, 1981.

[20] D. F. Brailsford and A. J. B. Robertson, "Calculation of electric field strengths at a sharp edge," *Int. J. Mass Spectrometry Ion Phys.*, vol. 1, no. 1, pp. 75–85, 1968, doi: 10.1016/0020-7381(68)80006-3.

[21] F. H. Kreuger, *Industrial High Voltage*. Delft, Netherlands: Delft Univ. Press, 1991.

[22] S. A. Madhar, "Defect identification through partial discharge analysis on HVDC: Partial discharge fingerprinting," Ph.D. dissertation, Delft Univ. Technol., Delft, Netherlands, 2021. [Online]. Available: http://resolver.tudelft.nl/uuid:052aa674-20a1-4af5-a543-52acf5c4f90b

[23] J. Jiang, W. Chen, Y. Song, and Z. Shen, "Active control strategy of partial discharge for insulation of high-power high-voltage high-frequency transformers (H^3Ts)," *IEEE Trans. Ind. Electron.*, vol. 70, no. 7, pp. 7521–7524, Jul. 2023, doi: 10.1109/TIE.2022.3203758.

[24] Z. Li, Y. Han, Z. Xie, H. Ren, Q. Li, and Z. Wang, "High-frequency partial discharge characteristics of solid-state transformer interturn multilayer insulation under repetitive electrical stress," *IEEE Trans. Ind. Electron.*, vol. 71, no. 10, pp. 13331–13340, Oct. 2024, doi: 10.1109/TIE.2024.3360614.

[25] R. Agarwal, H. Li, Z. Guo, and P. Cheetham, "The Effects of PWM with high *dv/dt* on partial discharge and lifetime of medium-frequency transformer for medium-voltage (MV) solid state transformer applications," *IEEE Trans. Ind. Electron.*, vol. 70, no. 4, pp. 3857–3866, Apr. 2023, doi: 10.1109/TIE.2022.3174243.

[26] J. Jiang, D. Cui, J. Liu, B. Chen, J. Chen, and R. Fu, "Partial discharge characteristics of epoxy resin under high-frequency pulse electrical stress," *IEEE Trans. Power Electron.*, vol. 40, no. 1, pp. 2017–2027, Jan. 2025, doi: 10.1109/TPEL.2024.3421624.

[27] X. Zhang et al., "Partial discharge measurement and analysis of transformer under oscillating lightning impulse voltage," *IEEE Trans. Dielectr. Electr. Insul.*, vol. 29, no. 6, pp. 2303–2311, Dec. 2022, doi: 10.1109/TDEI.2022.3205291.

[28] *IEEE Recommended Practice for the Detection of Partial Discharge and the Measurement of Apparent Charge in Dry-Type Transformers*, IEEE Standard C57.124-1991, 1991, doi: 10.1109/IEEESTD.1991.9131414.

[29] A. Ku¨chler, *High Voltage Engineering : Fundamentals – Technology – Applications*, [English] ed. Berlin, Germany: Springer-Verlag, 2018, doi: 10.1007/978-3-642-11993-4.

[30] S. Ganesan, "Feasibility analysis of synthetic air as a substitute for SF6 inside dielectric coated GIS," M.Sc. thesis, Delft Univ. Technol., Delft, The Netherlands, 2023. [Online]. Available: http://resolver.tudelft.nl/uuid:257ddaef-23f0-49bd-b321-610992c0330f

[31] D. Cottet et al., "Integration technologies for a medium voltage modular multi-level converter with hot swap capability," in *Proc. IEEE Energy Convers. Congr. Expo.*, 2015, pp. 4502–4509, doi: 10.1109/ECCE.2015.7310295.

[32] F. H. Kreuger, *Industrial High Voltage*. Delft, Netherlands: Delft Univ. Press, 1995.

[33] "Energy-epp0500 power cable accessories - South East Europe," 2015. Accessed: Nov. 12, 2024. [Online]. Available: https://www.scribd.com/document/359218105/energy-epp0500-PowerCableAccessories-SouthEastEurope-pdf

[34] *High-Voltage Test Techniques - Partial Discharge Measurements*, Standard IEC 60270:2000, International Electrotechnical Commission, Geneva, Switzerland, 2000.